Supporting Information

Hodgkins et al. 10.1073/pnas.1314641111

SI Materials and Methods

Sampling. Nine sites (Table 1 and Table S1) spanning the thaw progression from collapsed palsa to fen were selected for study. Between June 13 and June 16, 2011, peat was gathered with an 11-cm-diameter homemade circular push corer at all sites except the PHS and Fen1 sites, at which peat was gathered with a 10 cm × 10-cm square Wardenaar corer (Eijkelkamp). All sites were cored singly except S and E, which were cored in triplicate to capture spatial heterogeneity. Cores were divided into sections 3–10 cm thick, and the sections were placed into plastic bags and stored at 4 °C (the approximate peat temperature in the field) until analysis.

Before coring, pore water for pH and Fourier transform ion cyclotron resonance mass spectrometry (FT-ICR MS) was collected in the field by suction through a home-built 0.5-cm-diameter stainless steel tube connected to a 60-mL plastic syringe. pH was measured on-site with an Oakton Waterproof pHTestr 10 (Eutech Instruments). For FT-ICR MS, pore water was filtered through 0.7-μm Whatman GF/F glass microfiber filters into amber polycarbonate bottles and frozen within 8 h of collection until analysis.

Incubations. From each core, a section of surficial peat below the water table (Table S1) was selected for incubation. Three replicates were prepared for each site except for Fen1, which only had enough peat for two replicates. For sites with triplicate cores (S and E), each incubation replicate was taken from a separate core replicate, so the averages and SEs from these sites correspond with the averages and SEs across all three cores.

For each incubation replicate, 12–20 g of peat was placed in preweighed 100-mL borosilicate glass serum bottles (Wheaton, part number 223747) (actual volume to neck ∼120 mL), weighed, and covered with 40 mL of deionized water that had previously been degassed by bubbling N_2 through the water for 20 min. The final volume of peat plus water was enough to leave about 50–65% headspace volume in the bottles. The bottles were capped with 20-mm blue chlorobutyl septum stoppers (Bellco Glass, part number 2048–11800) and crimped with Supelco aluminum crimp seals (Sigma-Aldrich, part number 27230-U). Each vial had the headspace flushed with N_2 for 30 s, was shaken for 30 s, and had the headspace flushed again for 30 s. We performed a 25-d preincubation of vials in the dark at 22 °C to allow microbial elimination of any remaining oxygen or other electron acceptors introduced during processing, thus establishing methanogenic conditions. At the end of the preincubation, any CH_4 and CO_2 produced during the preincubation were removed by shaking the vials and flushing them with N_2 until additional shaking and flushing caused no further reduction in CH_4 and CO_2 concentrations. This procedure entailed shaking and flushing each vial a total of 5 times (30 s for each shaking, 30 s for the first two flushings, 60 s for the third flushing, and 3 min for the final two flushings), with maximum removal achieved after the first three shakings and flushings. Concentrations were determined by analysis on a Shimadzu GC-8A gas chromatograph with a methanizer and a flame ionization detector. After maximum removal, headspace CH_4 and CO_2 concentrations were <0.1% and <0.5% by volume, respectively; these concentrations were small compared to the later buildup in CH_4 and CO_2 during the main incubations (Fig. S1 *A*–*D*). At the end of the final flushing, enough N_2 was left in each vial to create a headspace pressure of 5–7 psi above atmospheric pressure as determined by a home-built needle-insertion pressure gauge. The end of the final flushing was defined as the incubation start time.

Vials were incubated at 22 °C in the dark for 62 d. One day following the incubation start date, and at least every 14 d thereafter, the headspace was analyzed for CH_4 and CO_2 concentrations and $\delta^{13}C$. Before each measurement, the incubation vials were shaken for 30 s, and the headspace pressures were measured. For determination of CH_4 and CO_2 concentrations and $\delta^{13}C$, headspace subsamples between 10 and 250 μL (depending on concentration) were directly injected into a continuous-flow Hewlett-Packard 5890 gas chromatograph (Agilent Technologies) at 35 °C coupled to a Finnigan MAT Delta S isotope ratio mass spectrometer via a Conflo IV interface system (Thermo Scientific) (GC-IRMS). Stable carbon isotope ratios ($^{13}C/^{12}C$) were expressed as $\delta^{13}C$ relative to the Pee Dee Belemnite (PDB) standard, where $\delta^{13}C = (R_{sample}/R_{standard} - 1) \times 1000$, and R_{sample} and $R_{standard}$ are the $^{13}C/^{12}C$ ratios in the sample and the PDB standard, respectively.

At the end of the incubation period and immediately following the final CH_4 and CO_2 analysis, samples were acidified with 2 mL of degassed 20% H_3PO_4 (excess) so that any dissolved inorganic carbon (DIC) that was still in the liquid phase could enter the headspace, and the samples were then analyzed again so that any changes in headspace CO_2 concentration or $\delta^{13}C$ could be determined. Acidification increased the headspace CO_2 concentration by >1% (the average relative error of the GC-IRMS concentration measurements) in only six of the incubations, all of them sedge fen peat with pH ≥ 5.7; consequently, a single replicate was measured for each of the bog and collapsed palsa sites (all of which had pH ≤ 4.2). Incubations that experienced no significant change in headspace CO_2 concentration (≤1%) with acidification also experienced negligible change in $\delta^{13}C_{CO2}$ (≤0.5‰). However, among the incubations that experienced >1% increase in headspace CO_2 concentration with acidification, $\delta^{13}C_{CO2}$ values also increased by up to 1.7‰.

Following the postacidification analysis of changes in CO_2 concentrations and $\delta^{13}C$, the sample vials were uncapped, dried at 60 °C until completely dry (∼60 d), and weighed.

Incubation Calculations. For CH_4, the total amount in the vial equals the amount of CH_4 in the headspace (based on an ideal gas law calculation) plus the amount of dissolved CH_4, which is calculated based on Henry's law:

$$n_{CH_4} = \frac{\chi_{CH_4} P (V_{vial} - V_{water})}{RT} + \chi_{CH_4} P V_{water} k_H, \qquad [S1]$$

where n_{CH_4} is the total amount of CH_4 in the vial (mol); χ_{CH_4} is the mole fraction in the headspace; P is the headspace pressure (atm); V_{vial} is the total vial volume (L); V_{water} is the volume of the combined peat and water (L), which is assumed (for simplification) to be mostly water; R is the gas constant ($L \cdot atm \cdot mol^{-1} \cdot K^{-1}$); T is the ambient temperature (K); and k_H is the Henry's law constant for CH_4 ($mol \cdot L^{-1} \cdot atm^{-1}$).

For CO_2, due to the complexity of the CO_2/DIC system, an "extraction efficiency" was defined as the proportion of inorganic carbon (as CO_2) in the headspace relative to the total inorganic carbon (DIC plus CO_2 gas) in the entire vial (1). The portion of this extraction efficiency affected by water volume alone, i.e., the extraction efficiency after acidification, was assumed to be proportional to the fractional volume of headspace in the jar. An exact relationship between fraction of headspace volume and the volume component of extraction efficiency (E_V) was determined by addition of 2 mM $NaHCO_3$ in volumes equal

to 25%, 50%, and 75% of the total vial volume to sealed vials with a headspace of N_2 at atmospheric pressure, followed by addition of excess H_3PO_4 and measurement of headspace CO_2 concentrations by GC-IRMS. This determination resulted in the following relationship:

$$E_V = -0.8057\left(\frac{V_{water}}{V_{vial}}\right) + 0.8458. \quad \textbf{[S2]}$$

In addition to the volume effect, acidification was required to extract the CO_2 into the headspace of some of the incubations with full efficiency, but the incubations were not acidified until the end of the incubation period. Therefore, the CO_2 concentrations measured over the course of the incubations had to be corrected for a pH component of extraction efficiency in addition to the volume component. The pH component of the extraction efficiency (E_{pH}) is defined as

$$E_{pH} = \frac{n^{before}_{CO_2,HS}}{n^{after}_{CO_2,HS}}, \quad \textbf{[S3]}$$

where $n^{before}_{CO_2,HS}$ is the amount of CO_2 in the headspace before acidification (mol) and $n^{after}_{CO_2,HS}$ is the amount of CO_2 in the headspace after acidification (mol). Although the incubations were only acidified on the final day, the pH of selected incubations was measured before acidification and found to be close to the in situ pH measured in the field, so E_{pH} was assumed to be constant throughout the incubation period. The value $E_{pH} = 1$ was used for the incubations that experienced no significant change in headspace CO_2 concentration after acidification. The total extraction efficiency for CO_2 (E_{total}) is the product of the volume and pH components,

$$E_{total} = E_V E_{pH}, \quad \textbf{[S4]}$$

and the total amount of inorganic carbon in the entire vial (n_{CO_2}) is then the amount of CO_2 in the headspace (calculated analogously to the amount of headspace CH_4) divided by the total extraction efficiency:

$$n_{CO_2} = \frac{\chi_{CO_2} P(V_{vial} - V_{water})}{RT}\frac{1}{E_{total}}. \quad \textbf{[S5]}$$

In addition to the effect of pH on the total CO_2 extraction efficiency, pH also had a slight effect on the measured $\delta^{13}C_{CO2}$ values. Therefore, in addition to the correction for $E_{pH} < 1$, these incubations were also corrected to account for these shifts in $\delta^{13}C_{CO2}$ with acidification:

$$\delta^{13}C^{corr}_{CO_2} = \delta^{13}C^{meas}_{CO_2} + \left(\delta^{13}C^{after}_{CO_2} - \delta^{13}C^{before}_{CO_2}\right), \quad \textbf{[S6]}$$

where $\delta^{13}C^{corr}_{CO_2}$ is the corrected value, $\delta^{13}C^{meas}_{CO_2}$ is the measured value, $\delta^{13}C^{after}_{CO_2}$ is the measured value after acidification, and $\delta^{13}C^{before}_{CO_2}$ is the measured value before acidification.

Measured amounts and $\delta^{13}C$ of CH_4 and CO_2 over the incubation period are shown in Fig. S1. CH_4 and CO_2 production rates were calculated based on linear regressions of molar amount (corrected for extraction efficiency) per gram of dry peat vs. time. To quantify changes in CH_4 and CO_2 production along the thaw progression, we assigned numbers 1–9 to the sites based on the hypothesized order of the thaw succession (Table 1 and Table S1) and performed linear regressions on the base-10 logarithms of the CH_4 and CO_2 production potentials and ratios in the individual incubation replicates vs. thaw position (Fig. S2). The logarithms of the production potentials were used due to the nonlinearity of the increase in gas production rates with thaw (Fig. 1 *A* and *B*), and the logarithms of CH_4/CO_2 ratios were used because the ratio of two exponential functions is also exponential. Statistical significance was tested based on the correlation coefficients (R^2) of the regressions, and all increases were found to be significant with $P < 0.0001$.

Overall $\delta^{13}C_{CH4}$ and $\delta^{13}C_{CO2}$ for the incubation period (Fig. 2 *A* and *B*) were defined as the acidification-corrected $\delta^{13}C_{CH4}$ and $\delta^{13}C_{CO2}$ on day 62 (which represent integrated $\delta^{13}C$ of all gas production during the incubations), and α_C values (2) were calculated based on these corrected final $\delta^{13}C$ values. The incubations appeared to fall into two groups based on α_C (Fig. 2*C*): group 1 consisting of collapsed palsas and bogs ($\alpha_C = 1.085 \pm 0.001$), and group 2 consisting of all fens ($\alpha_C = 1.052 \pm 0.001$). Based on an independent two-sample unpaired *t* test, the groups were significantly different with $t(24) = 16.5564$ and $P < 0.0001$.

C/N ratios. Five to 10 g of each peat core section was weighed, dried at 60 °C until completely dry (3–10 d), weighed again, and ground to a fine powder. For each peat depth, two subsamples—one 80–100-μg subsample for C analysis and one 5,000–6,000-μg subsample for N analysis—were wrapped in tin capsules. Samples were analyzed by combustion to CO_2 and N_2 at 1,020 °C in an automated CHN elemental analyzer coupled with a Thermo-Finnegan Delta XP isotope ratio mass spectrometer. Samples were run in nondilution mode for carbon analysis and dilution mode (×10) for nitrogen analysis.

Results were obtained in the form of %C and %N (by weight), and the C/N ratios were calculated as the ratio of %C/%N for corresponding pairs of subsamples.

FTIR Spectroscopy. Spectral characterization of peat samples was performed by diamond attenuated total reflectance FTIR spectroscopy on a PerkinElmer Spectrum 100 FTIR spectrometer fitted with a CsI beam splitter and a deuterated triglycine sulfate detector. An attenuated total reflectance (ATR) accessory made from a composite of zinc selenide and diamond, with a single reflectance system, was used to produce transmission-like spectra. Peat samples were first dried in an oven at 60 °C until completely dry (3–10 d), then ground to a fine powder. Samples were then placed directly on the crystal and force was applied to ensure good contact between the crystal and the sample. Spectra were acquired by averaging 50 scans at 4-cm^{-1} resolution (wavenumber) over the range 4,000–650 cm^{-1}. The spectra were corrected for the ATR to allow for differences in depth of beam penetration at different wavelengths, and then baseline corrected, with the instrument software.

To calculate humification indices, we calculated ratios between absorbances at the following wavenumbers with respect to polysaccharides (1,030 cm^{-1}): 2,920, 2,850, 1,630, and 1,515 cm^{-1} (3–6) (functional group assignments for each wavenumber are given in Fig. 4*B*). Beer et al. (5) and Broder et al. (6) define the polysaccharide and aromatic C=C/amide C=O wavenumbers as 1,090 cm^{-1} and 1,510 cm^{-1}, respectively, but the corresponding absorption maxima in our samples occur closer to 1,030 cm^{-1} and 1,515 cm^{-1}.

FT-ICR MS. A custom-built FT-ICR mass spectrometer with 9.4-T superconducting magnet located at the National High Magnetic Field Laboratory (NHMFL) was used to collect ultrahigh resolution mass spectra in two selected pore water samples: one from the SOS site at 31 cm, and one from the E site at 25.5 cm. The use of this instrument to determine the composition of complex natural dissolved organic matter in peatland porewaters has been described in detail (7, 8). Briefly, a solution containing the dissolved organic matter (DOM) in methanol was prepared for each selected sample by solid phase extraction (9) so that the final concentration was 500 mg C/mL. Samples were then introduced

to an electrospray ionization source through a syringe pump at a flow rate of 0.5 μL/min that was equipped with a 50-μm i.d. fused silica tube (10, 11). Two hundred individual scans were summed and the average resolving power (m/Dm 50%) was >700,000 at 451 Da. Spectra were calibrated by two internal series of DOM homologous series separated by 14 Da ($-CH_2$ groups) and the mass accuracy was calculated to be <1 ppm for singly charged ions ranging across the mass spectral distribution (m/z 300–900). NHMFL MS software was used to calculate all possible molecular formulas within a ±1-ppm error taking into consideration the presence of C, H, O, N, and S (12). All observed ions were singly charged as confirmed by the 1.0034-Da spacing found between isotopic forms of the same molecule (between $^{12}C_n$ and $^{12}C_{n-1}{}^{13}C_1$) (13, 14).

1. Corbett JE, et al. (2013) Partitioning pathways of CO_2 production in peatlands with stable carbon isotopes. *Biogeochemistry* 114(1-3):327–340.
2. Whiticar MJ, Faber E, Schoell M (1986) Biogenic methane formation in marine and freshwater environments: CO_2 reduction *vs.* acetate fermentation—Isotope evidence. *Geochim Cosmochim Acta* 50(5):693–709.
3. Holmgren A, Nordén B (1988) Characterization of peat samples by diffuse reflectance FT-IR spectroscopy. *Appl Spectrosc* 42(2):255–262.
4. Niemeyer J, Chen Y, Bollag J-M (1992) Characterization of humic acids, composts, and peat by diffuse reflectance Fourier-transform infrared spectroscopy. *Soil Sci Soc Am J* 56(1):135–140.
5. Beer J, Lee K, Whiticar M, Blodau C (2008) Geochemical controls on anaerobic organic matter decomposition in a northern peatland. *Limnol Oceanogr* 53(4):1393–1407.
6. Broder T, Blodau C, Biester H, Knorr KH (2012) Peat decomposition records in three pristine ombrotrophic bogs in southern Patagonia. *Biogeosciences* 9(4):1479–1491.
7. Tfaily MM, Podgorski DC, Corbett JE, Chanton JP, Cooper WT (2011) Influence of acidification on the optical properties and molecular composition of dissolved organic matter. *Anal Chim Acta* 706(2):261–267.
8. Tfaily MM, et al. (2013) Investigating dissolved organic matter decomposition in northern peatlands using complimentary analytical techniques. *Geochim Cosmochim Acta* 112:116–129.
9. Tfaily MM, Hodgkins S, Podgorski DC, Chanton JP, Cooper WT (2012) Comparison of dialysis and solid-phase extraction for isolation and concentration of dissolved organic matter prior to Fourier transform ion cyclotron resonance mass spectrometry. *Anal Bioanal Chem* 404(2):447–457.
10. Chowdhury SK, Katta V, Chait BT (1990) An electrospray-ionization mass spectrometer with new features. *Rapid Commun Mass Spectrom* 4(3):81–87.
11. Senko MW, et al. (1996) Electrospray ionization Fourier transform ion cyclotron resonance at 9.4 T. *Rapid Commun Mass Spectrom* 10(14):1824–1828.
12. Stenson AC, Marshall AG, Cooper WT (2003) Exact masses and chemical formulas of individual Suwannee River fulvic acids from ultrahigh resolution electrospray ionization Fourier transform ion cyclotron resonance mass spectra. *Anal Chem* 75(6): 1275–1284.
13. Brown TL, Rice JA (2000) Effect of experimental parameters on the ESI FT-ICR mass spectrum of fulvic acid. *Anal Chem* 72(2):384–390.
14. Kujawinski EB, Hatcher PG, Freitas MA (2002) High-resolution Fourier transform ion cyclotron resonance mass spectrometry of humic and fulvic acids: Improvements and comparisons. *Anal Chem* 74(2):413–419.

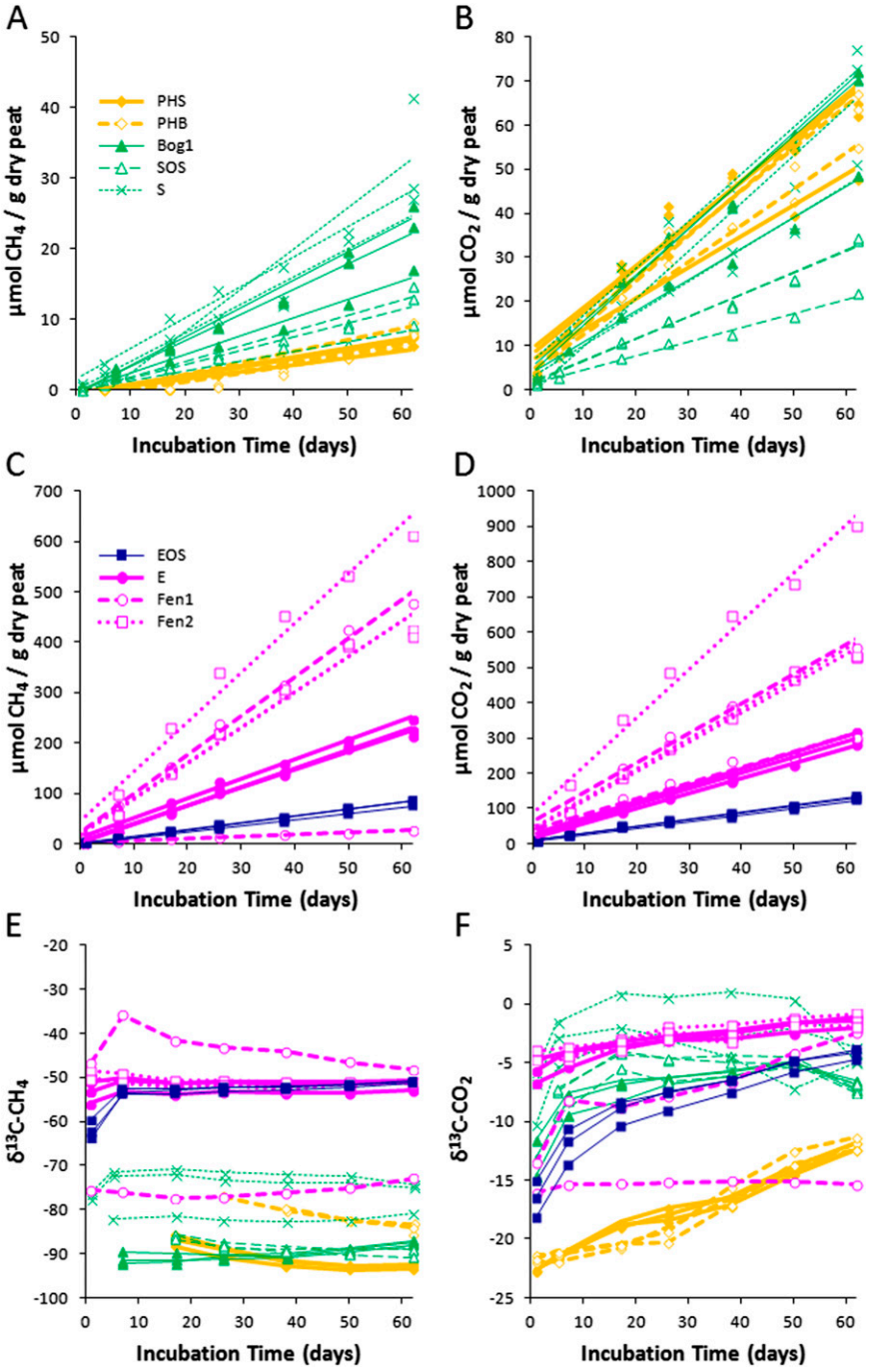

Fig. S1. Cumulative amounts and $\delta^{13}C$ of CH_4 and CO_2 produced in incubations. (*A–D*) Amounts of CH_4 and CO_2 produced in peat from collapsed palsas (gold: PHS, PHB), bogs (green: Bog1, SOS, S), fens with *Sphagnum* spp. and sedges (dark blue: EOS), and fens with sedges only (pink: E, Fen1, Fen2), overlaid with linear fits used to calculate gas production rates (R^2 = 0.84–1.00). Lines of the same style represent incubation replicates. (*E* and *F*) $\delta^{13}C$ of CH_4 and CO_2 in all incubations, connected with lines to show overall trends (same marker and line styles as *A–D*). Within-sample error bars are smaller than the marker sizes.

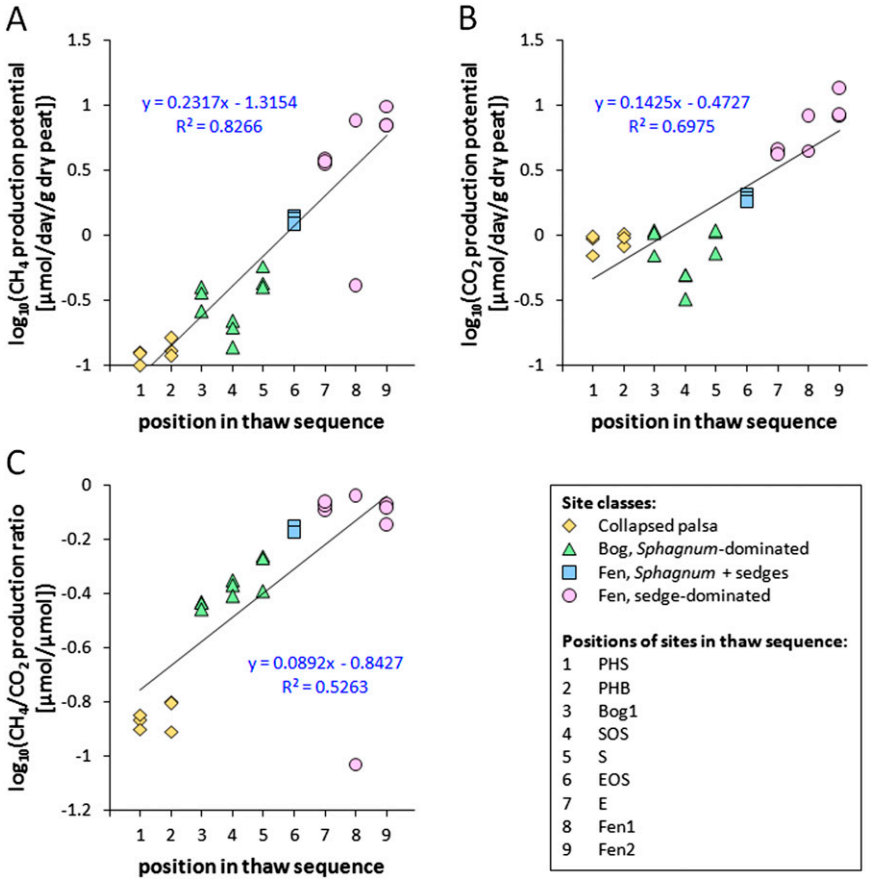

Fig. S2. Log-linear regressions of incubation-derived gas production potentials vs. position in the thaw sequence: (*A*) CH_4 production potential, (*B*) CO_2 production potential, and (*C*) CH_4/CO_2 production ratio. "Position in thaw sequence" is defined as the approximate order of time since permafrost thaw for the sites used in this study (see the first footnote in Table S1).

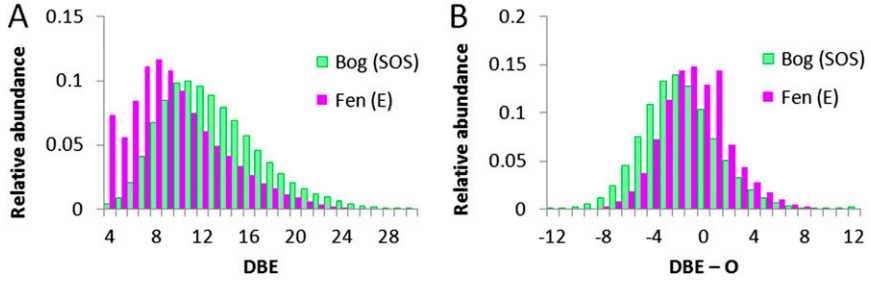

Fig. S3. Abundance distributions of compounds in DOM as a function of double-bond equivalence (DBE) and DBE–O. The leftward shift of the bog (site SOS, 31 cm) relative to the fen (site E, 25.5 cm) distribution between (*A*) DBE and (*B*) DBE–O, together with bog DOM's higher O/C ratios (Fig. 5*A*), indicates higher oxygen content in bog DOM. This result signifies that bog DOM has a higher oxidation state than fen DOM.

Table S1. Sites selected for study, in approximate order of thaw stage

Site name*	Habitat classification	Dominant vegetation	pH‡	WTD, cm§	Thaw depth, cm¶	"Surface" depths used for incubations, cm	Notes
PHS	Collapsed palsa	*Eriophorum vaginatum*, woody species	4.1	0	>90	9–12	Smaller thermokarst sinkhole.
PHB	Collapsed palsa	*E. vaginatum*, floating *Sphagnum*	4.1	>0	>90	10–15	Larger thermokarst sinkhole.
Bog1	Bog	*Sphagnum* spp.	4.2	−17	25	18–22	Elevation close to surrounding palsa.
SOS	Bog	*Sphagnum* spp.	4.0	−12	34	12–17	Intermediate between Bog1 and S.
S (triplicate cores)†	Bog	*Sphagnum* spp.	4.2	−12 to −13	30–31	12–16	Thawed much deeper than Bog1 or SOS in August 2012.
EOS	Fen	*Eriophorum angustifolium*, *Sphagnum* spp.	4.8	5	44 to >90	5–10	Sporadic, thin frozen layer at 44 cm.
E (triplicate cores)†	Fen	*E. angustifolium*	5.8	0–4.5	27 to >90	5–8	Usually thaws completely by August.
Fen1	Fen	*Carex rostrata*	6.0	6–8	>90	5–8	Usually thaws completely by August.
Fen2	Fen	*E. angustifolium*	5.7	12	>90	0–10	Usually thaws completely by August.

Expanded from Table 1 to include water table depth (WTD), thaw depth, depths used for incubations, and additional information.

*Order of sites determined by habitat classification (see main text), vegetation, active layer depth, WTD, and in the case of fens, distance from the nearest lake (Lake Villasjön), which has been gradually increasing in size with the thaw of surrounding permafrost.

†CH_4 and CO_2 fluxes (1) have previously been measured with an autochamber system at these sites.

‡Average pore water pH between 0 and 32 cm below peat surface. Within this depth range, pH did not show any appreciable trends with depth. SEs ≤ 0.15 pH units.

§Positive numbers indicate water above the peat surface (most common sign convention for WTD, which is opposite of other depths indicated).

¶Thaw depth at time of sampling. Actual active layer, which includes seasonally frozen peat, is thicker.

1. Bäckstrand K, et al. (2010) Annual carbon gas budget for a subarctic peatland, Northern Sweden. *Biogeosciences* 7:95–108.

Table S2. Humification indices (HI) of (*A*) surface peat from <10 cm, (*B*) near-surface peat from depths used in incubations (Table S1), and (*C*) deep peat from 24 to 35 cm.

Site	Depth, cm	2,920/1,030	2,850/1,030	1,630/1,030	1,515/1,030
Surface core sections, <10 cm					
PHS	1–4	0.64	0.52	0.53	0.20
PHB	0–5	0.54	0.43	0.34	0.11
Bog1	0–4	0.44	0.32	0.26	0.09
SOS	0–6	0.48	0.36	0.28	0.09
S	1–4	0.43	0.34	0.24	0.09
EOS	0–5	0.64	0.47	0.59	0.30
E	1–4	0.76	0.56	0.70	0.40
Fen1	1–4	0.42	0.32	0.36	0.18
Fen2	0–10*	0.57	0.45	0.44	0.21
Near-surface core sections, Table S1; used in incubations					
PHS	9–12	0.56	0.42	0.41	0.15
PHB	10–15	0.66	0.52	0.44	0.13
Bog1	18–22	0.48	0.37	0.33	0.13
SOS	12–17	0.45	0.36	0.26	0.09
S	12–16	0.51	0.40	0.34	0.14
EOS	5–10	0.88	0.67	0.71	0.33
E	5–8	0.64	0.48	0.55	0.28
Fen1	5–8	0.64	0.51	0.57	0.32
Fen2	0–10	0.57	0.45	0.44	0.21
Deep core sections, 24–35 cm					
PHS	30–33	0.56	0.43	0.48	0.20
PHB	25–30	0.78	0.61	0.49	0.21
Bog1	27–31	0.66	0.50	0.46	0.19
SOS	27–33	0.72	0.56	0.41	0.16
S	17–21†	0.57	0.42	0.36	0.15
EOS	25–30	1.09	0.86	0.88	0.47
E	24–27	0.57	0.41	0.42	0.21
Fen1	24–27	1.64	1.15	1.02	0.60
Fen2	30–35	0.86	0.71	0.75	0.41

Within-sample variability for all HI is ±0.01 (SE), based on parallel analysis of replicate samples collected at the same depth and time.

*Same as incubation sample.

†No samples were gathered deeper than 21 cm at this site. Because this section was from above 24 cm, these values are not shown in Fig. 3*B*.